Materials Research. 2021; 24(3): e20200482
DOI: https://doi.org/10.1590/1980-5373-MR-2020-0482

Effects of Stirring Time and Cooling Rate on the Rheocast Microstructure and Mechanical Properties of Magnesium Alloy MRI 230D

Igor Zimpel*[a], Sergio Luiz Telles Bartex[b], Vinicius Karlinski de Barcellos[a]

[a]*Universidade Federal do Rio Grande do Sul (UFRGS), Laboratório de Fundição (LAFUN), Porto Alegre, RS, Brasil.*
[b]*Centro Universitário Ritter dos Reis (UNIRITTER), Porto Alegre, RS, Brasil.*

Received: October 19, 2020; Revised: February 2, 2021; Accepted: March 14, 2021

Semisolid state processing is a methodology that transforms dendritic as-cast microstructure into globular non-dendritic microstructure with optimized mechanical properties. Rheocasting process involves mechanically stirring metals in a semisolid state and its benefits are associated with processing parameters. In order to evaluate stirring time effects, magnesium alloy MRI 230D (Mg–Al6.45–Ca2.25–Mn0.27–Sr0.25–Sn0.84) was melted and cooled down to semisolid processing temperature (595ºC). Moreover, isothermal stirring was executed for 1, 2, 4 and 8 minutes. In each experiment, cylindrical samples with different diameters (6 and 12 mm) were collected to evaluate cooling rates effects. The microstructure was analyzed through optical and electron microscopes. The results showed that in the longest stirring times, the primary α-Mg phase got coarser and the interglobular region became more refined. Although shape factor initially increased, subsequently there was a tendency to stabilize. Regarding cooling conditions, it was found that the interglobular region became more refined at higher cooling rates. Mechanical tests revealed an initial decrease in ultimate tensile strength (UTS) and ductility, but afterwards increased due to a more regular microstructure and superior shape factor. The 8-minutes stirring sample achieved the best results: an increase of 12% in UTS and 16% in ductility.

Keywords: *MRI 230D, magnesium, semisolid, rheocast, stirring time, cooling rate.*

1. Introduction

Magnesium alloys have an excellent weight/resistance ratio, high recycling capacity and low density. Based on these characteristics, in recent years the research and development of magnesium alloys for industrial application have increased significantly, replacing materials such as steel, aluminum and structural plastics. However, the deformability and toughness of magnesium alloys are generally lower than aluminum alloys and the hexagonal close-packed (HCP) crystal structure of magnesium alloys limits the deformation process. Furthermore, the application of magnesium alloys is limited due to their low creep resistance[1-3].

Many studies point out that the addition of alloying elements, such as Al, Ca and Rare Earth elements (mischmetal), was effective in improving the mechanical performance of Mg alloys at high temperatures. Even so, the problems of low toughness and deformability still remain. With that in mind, processing in a semisolid state has become of great interest in studies with magnesium alloys. The SSM (semisolid metal) processing can cause significant changes in the microstructure of materials such as shape factor, refining, primary particle distribution, among others. The purpose of SSM processing is to form a uniform and refined microstructure, with a high shape factor and improved mechanical properties, aiming at an increase in toughness and ductility. Therefore, the optimization of processing parameters becomes a possible solution to the problems found in Mg alloys[4-6].

Rheocasting is one of several methods to process metal alloys in a semisolid state. The main parameters of the process are stirring time, cooling rate, type of stirring, solid fraction and stirring speed and each of their variation directly affects the resulting microstructure[7,8]. The main spheroidization mechanism in the rheocasting process is the shear model, in which the dendritic arms are sheared and projected into the remaining liquid. The formation of spherical structures occurs not only as a result of the shear stress produced by stirring, but also due to the solute flow caused by the difference in solubility between the solid and the liquid and due to the spheroidal shape being the lowest free energy morphology in the system. Stirring is essential for the formation of a spherical structure and, if it is interrupted, it also discontinues spheroidization, which can lead to new dendritic formations from the already formed globules. Moreover, the Ostwald Ripening model is proposed to explain the growth behavior of the globules and it presents the mechanism of coalescence of spherical structures, in which larger globules grow at the expense of smaller ones due to the less surface energy. Although rheocasting is a low-cost process, it requires qualified labor and a strict control of the process[9,10].

The MRI 230D magnesium alloy was developed for die casting at high temperatures, exhibiting good mechanical and corrosion resistance, high creep resistance and low-cost. On the other hand, MRI 230D has low impact strength and low deformability when compared to commercial magnesium

* e-mail: ig_zi@hotmail.com

alloys. The main alloying elements are Al, Ca, Sr and Sn. Also, a low percentage of Mn is added in order to increase the corrosion resistance[3,11-13].

There are not many studies regarding the influence of semisolid processing on Mg alloys for high temperature applications. However, the SSM processing of commercial Al and Mg alloys has shown that the optimization of processing parameters such as cooling rate and stirring time positively affects the mechanical properties[6,9]. Thus, based on the characteristics of the MRI 230D alloy, this work aims to analyze the influence of cooling rates and stirring time on the microstructure and mechanical properties of the alloy when submitted to the rheocasting process.

2. Experimental

2.1 Solidification apparatus

A commercial ingot of the MRI 230D magnesium alloy provided by RIMA Industrial S/A was used with the nominal composition Mg–Al6.45–Ca2.25–Mn0.27–Sr0.25–Sn0.84.

The details of the experimental apparatus and the experimental procedures are described below. First, the magnesium ingots were melted in an electrical resistance furnace (4kW), with a protective atmosphere of pure Argon (5 L.min^{-1}). The furnace consisted of a SAE 420 stainless steel crucible with dimensions 240 x 118 mm (height and diameter). The furnace lid had access to the argon injection system, as well as to the tubes used for sample collection and for positioning the thermocouples, as shown in Figure1A. For each experiment, 1 kg of commercial alloy was melted.

2.2 Thermal analysis

In order to analyze the solidification range, in the first stage of the experiment the alloy was melted at 660°C, overheated to about 50°C, and slowly cooled to room temperature inside the furnace at a cooling rate of approximately 2.4°C.min^{-1}. Liquidus (T_L) and Solidus (T_S) temperatures were obtained through the CA-CCTA (Computer-aided Cooling Curve Thermal Analysis) method, a thermal analysis technique that relates the thermal changes on the cooling curve to phase transformations. A correlation between the inflection points on the cooling curve and its derivative allowed a better understanding of the transformations and reactions observed in a solidifying sample with the aid of thermocouples[14]. The temperature measurement and data acquisition were performed using type K thermocouples (1.6 mm diameter and error limit of ± 0.75%) with stainless steel sheath and 1 m length, using the National Instruments system (10 Hz) and with the aid of the LabView 6.2 software. For each experiment, two thermocouples were used: one positioned inside the furnace and another one inside the molten magnesium bath.

2.3 Solid fraction

The solid fraction is one of the main parameters of rheocasting, directly affecting the processed microstructure. Its recommended values are between 0.1 and 0.5[6,9,15]. In this study, a solid fraction was fixed in 0.25. The calculation of the solid fraction as a function of temperature was performed using the Scheil Equation (1942), which considers complete mixing in the liquid and absence of diffusion in the solid, where $\boldsymbol{fs = 1-(T_S-T_P/T_S-T_L)^{1/k-1}}$, $\boldsymbol{fs}$ represents the solid fraction ($0 < \mathbf{fs} < 1$), $\boldsymbol{T_L}$ the Liquidus temperature (612°C), $\boldsymbol{T_S}$ melting temperature of pure Mg (650°C), $\boldsymbol{T_P}$ the processing temperature (595°C) and $\boldsymbol{k}$ the partition coefficient (0.27), as used by several authors[4,16,17]. The partition coefficient was calculated from the Mg-Al phase diagram[6,7,15].

2.4 Cooling rate analysis

In the second stage of the experiments, the ingots (melted at 660°C) were cooled down to processing temperature

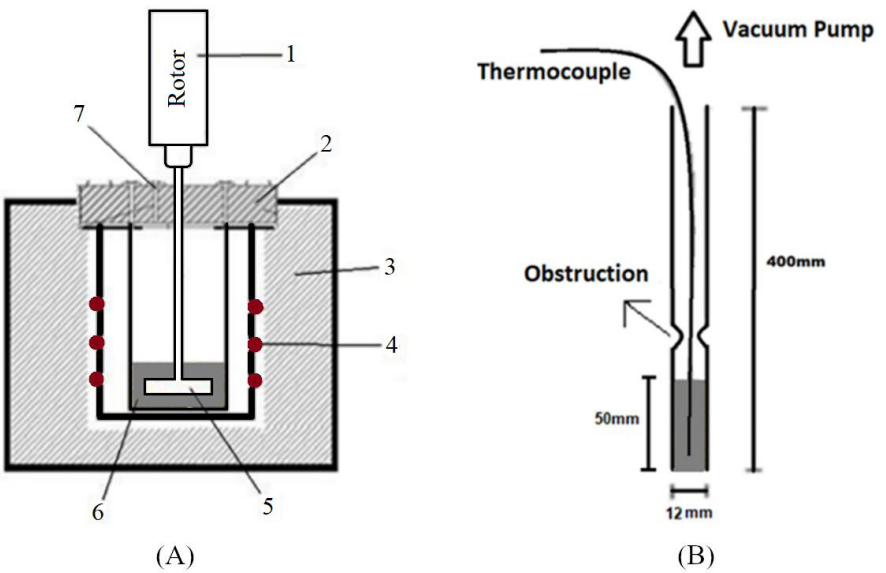

Figure 1. Scheme of the experimental apparatus, with detail of the tube for sample acquisition. (A) Electrical resistance furnace. (1) Rotor; (2) Furnace lid with access to stirring tool, thermocouples and the tubes; (3) Thermal insulation; (4) Electrical resistances; (5) Stirring tool (110 x 25 x 3 mm); (6) Liquid metal; (7) Argon injection access. (B) Scheme of the 12 mm tube.

595°C at a rate of 2.4°C.min^{-1}. At this temperature, the solid fraction was approximately 25% of solid (fs=0.25) for MRI 230D alloy. To analyze the cooling rate effect, samples were collected through steel tubes coupled to a vacuum pump (550W) - as showed in Figure 1B - and cooled as fast as possible in water (595 to 25°C). An obstruction on the back of the tube was made to prevent the passage of the liquid metal to the pump. To evaluate the different cooling rates, two different tubes were used with diameters of 6 and 12 mm, wall thickness of 1.2 mm and length of 400 mm. The tubes were preheated to 595°C.

2.5 Stirring time analysis

To analyze the effects of stirring time, mechanical stirring was performed by using a rotor attached to a stirring tool (paddle with two blades), with dimensions of 110 x 25 x 3 mm. The stirrer, preheated to 595°C before being introduced into the molten magnesium alloy, was coupled to an electric motor (3/4 HP) with the stirring speed set to 950 rpm. The samples were collected in the following stirring times: 0, 1, 2, 4 and 8 minutes. The 0-minute stirring time means that magnesium slurry was not stirred.

A control sample (CS) with zero solid fraction (at 612°C) and unprocessed was also collected and used to compare with the processed samples (595ºC) in the semisolid state. In this condition, the CS represented the alloy solidifying from the liquid state with a constant cooling rate, as close as possible to the cooling rates of the processed samples, resulting in a typical as-cast structure formation.

For each experiment (CS, 0, 1, 2, 4 and 8 min), 4 samples were collected, totalizing 48 samples (24 for each diameter – 6 and 12 mm), and later used for microstructure and mechanical analysis. In addition, 3 samples (0-minute) of each diameter were instrumented with thermocouples to acquire the cooling rates. The experimental parameters used in the processing are summarized in Table 1. The stirring speed, the temperature of the cooling water and the type of agitation (mechanical) were kept constant.

2.6 Microstructural analysis

After cooling, the samples were sectioned transversely and longitudinally for further metallographic analysis. Etching was carried out with Nital 1% for 3 seconds. The sections were inspected using an optical microscope model BX60M-OLYMPUS and a scanning electron microscope (SEM) model XL30- PHILIPS, coupled to an Energy Dispersive Spectrometry (EDS). ImageJ software version 1.51n was used to analyze the images. The thermal cycle applied in the experiment was carried out as indicated in Figure 2.

The α-Mg grain is an important factor for the analysis of the microstructure, strength being influenced by morphology and grain size. In cast (or rheocast) components, the secondary dendrite arm spacing (SDAS) is another influential parameter on the yield strength. In general, an understanding of the morphology, distribution and size of the different phases is important as they directly influence the mechanical behavior. The fraction and type of pores or defects are also of great relevance[18,19].

The shape factor (SF) is an important tool in materials science to understand the relationship between microstructure and mechanical properties. The sphericity, used to evaluate the most significant globules, is given by $\boldsymbol{SF = (4\pi A)/p^2}$ where $\boldsymbol{SF}$ is the shape factor, $\boldsymbol{A}$ the area of the primary α-Mg phase and $\boldsymbol{p}$ the perimeter[19,20].

The effects of the cooling rate on the remaining interglobular microstructure were analyzed through the measurement

Table 1 - Experimental data of the rapidly cooled samples.

Experiment	Stirring time	Temperature (°C)	Solid fraction
CS	0-minute	612°C	0%
0 min	0-minute	595°C	25%
1 min	1-minute	595°C	25%
2 min	2-minutes	595°C	25%
4 min	4-minutes	595°C	25%
8 min	8-minutes	595°C	25%

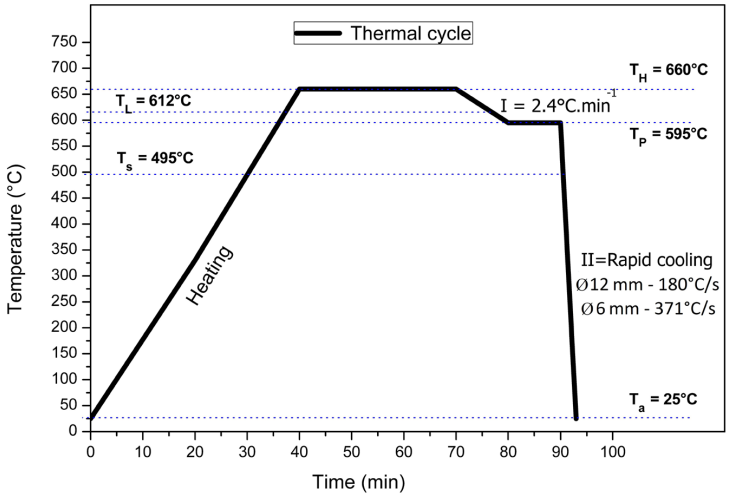

Figure 2. Thermal cycle applied in the processing. T_H-Overheating temperature; T_L-Liquidus temperature; T_P-Processing temperature. Ts-Solidus temperature. T_a-Room temperature. (I) Slow cooling. (II) Rapid cooling.

of SDAS, commonly used to evaluate the microstructure refinement[21,22]. It is measured by the linear interception method, which is based on the average length between the adjacent arms (secondary branches), represented by ***SDAS = L/(n-1),*** where ***L*** is the center-to-center distance of the secondary dendritic arm spacing and ***n*** is the number of branches.

2.7 Mechanical tests

Mechanical tests were performed on samples acquired from each experimental condition. They were machined according to the ASTM B557-15 standard. Four samples of each condition were tested. The tensile tests were performed using the universal testing machine Emic DL500B. In addition, the fracture surface of the MRI 230D alloy was analyzed with the aid of a scanning electron microscope (SEM).

3. Results and Discussion

3.1 Thermal analysis

The thermal analysis was performed in two stages: at first the slow cooling curves were collected (Figure 3A) in order to obtain the solidification range and the phase transformations of the MRI 230D alloy. In the second stage, the rapid cooling curves were obtained (Figure 3B) to verify the variation in the cooling rate between samples with different diameters (6 and 12 mm).

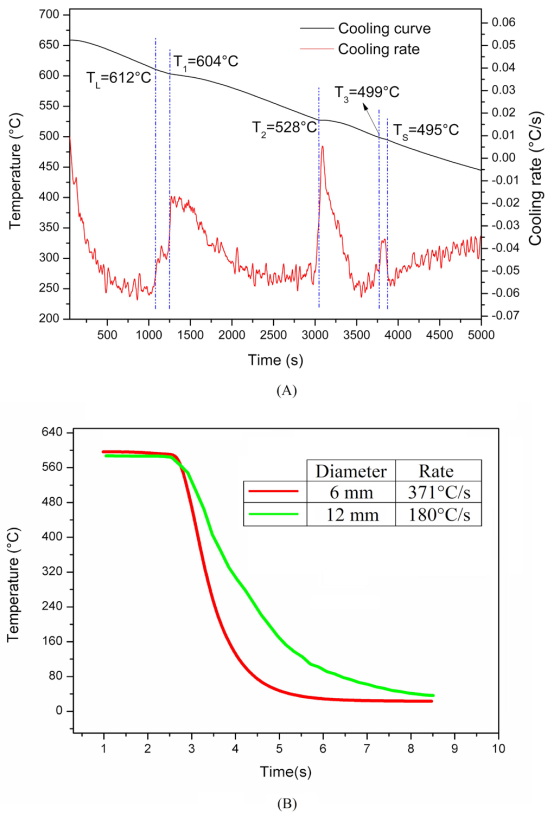

Figure 3. Thermal analysis of the experiment. (A) Correlation between the cooling curve and the cooling rate. (B) Rapid cooling curves, in detail the average cooling rates.

Figure 3A (first stage) shows the thermal evolution of the slow cooling condition sample (rate of 2.4°C.min^{-1}) and its phase transformation temperatures. The blue dashed lines indicate the temperatures of each inflection point in the slow cooling curve. The solidification starts at 612°C (T_L), with three further phase transformations at 604°C (T_1), 528°C (T_2) and 499°C (T_3). Finally, at 495°C (T_S), the solidification ends. According to JANZ (2008) and other authors[11,12,23,24] that have studied the phase transformations of the MRI 230D alloy, the solidification starts with the formation of the intermetallic Al-Mn. After, the magnesium matrix (α-Mg) at temperatures slightly above 600°C is formed. Around T_2, the Al-Ca-Sr phases begins to form. Finally, the last intermetallic phases, resulting from the supersaturation of Sn and Mn in liquid phase, form the remaining Al-Mn and Mg-Sn particles, at approximately T_3. The solidification ends around 500°C. The temperatures found were similar. Moreover, distinctions in transformation temperatures when compared to the ones found in literature may be due to the difference in the chemical composition of alloys or accuracy of the thermocouples.

Figure 3B (second stage) shows the rapid cooling curves obtained in the experiment, in detail the cooling rates, 371°C.s^{-1} ± 18 for the 6 mm sample and 180°C.s^{-1} ± 13 for the 12 mm sample. Only the solidification range was considered for the calculation. The cooling rates obtained were very high for both sample diameters, even though there was a significant difference between them: a reduction of approximately 52%. High cooling rates are recommended in order to freeze the microstructure obtained in processing[6,10].

3.2 Stirring time analysis

It is known that the rheocasting process aims to transform the primary dendritic phase into a globular structure. Figure 4 shows the morphological evolution of the 6 mm diameter samples submitted to different experimental conditions. Figure 4A and B correspond to the unprocessed samples with zero percent of solid fraction (CS) in different magnifications. Figure 4C, the non-stirred samples with 25% percent solid fraction (0 min). And Figure 4D, the 1-minute processed samples.

The unprocessed sample (Figure 4A and B) presents a refined dendritic microstructure. The non-stirred semisolid sample, Fig-4C, exhibits an irregular and coarser dendritic primary α-Mg phase and a refined dendritic microstructure in the remaining region. The processed sample (Figure 4D), stirred for 1 minute, shows a more regular primary α-Mg phase tending to form a globular morphology, as well as a refined microstructure in the remaining region, presenting both dendritic and globular morphologies. This occurred due to the rapid cooling of the semisolid slurry, that froze the microstructure obtained in the processing. In the remaining region, it is possible to observe the formation of refined dendritic structures due to the high cooling rate to which the material was submitted after processing. However, in Figure 4D, there was also the formation of refined globular structures: some particles, sheared in mechanical stirring, were projected in the liquid matrix, forming in the remaining region both dendrites and globular structures. It is also possible to observe shrinkage porosity formed due to the

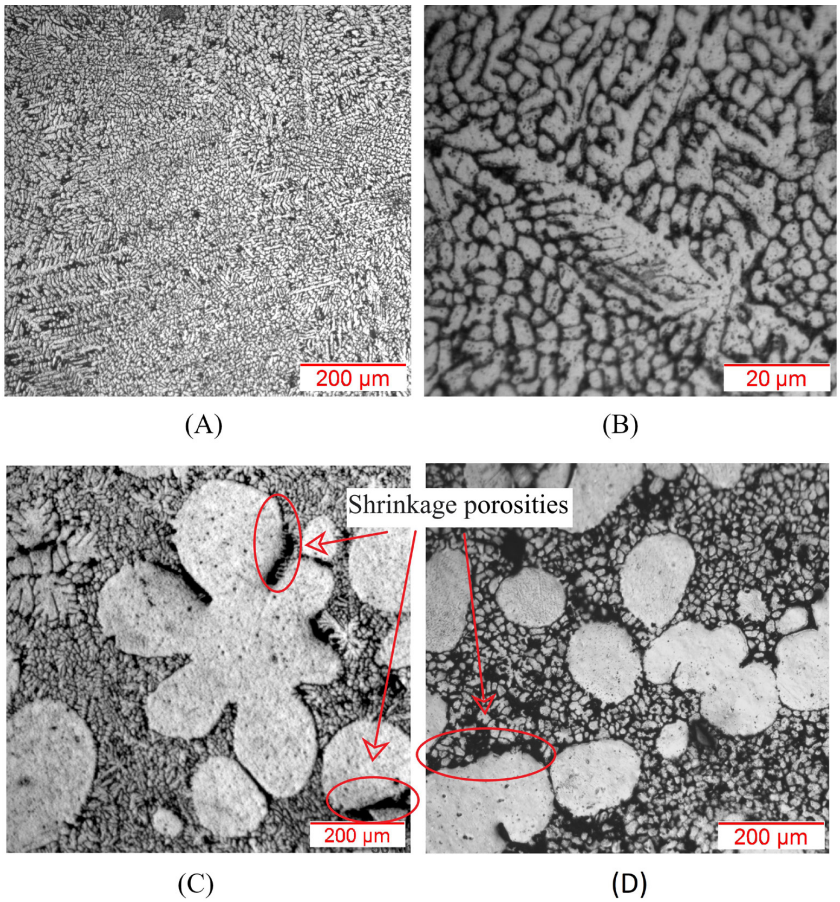

Figure 4. Microstructure of the 6 mm samples: (A) and (B) Unprocessed sample with zero percent solid fraction in different magnifications (CS sample); (C) Non-stirred sample with 25% percent solid fraction (0-minute sample); (D) Processed sample (1-minute sample).

higher viscosity of the semisolid as well as the difference in volumetric contraction between the solid and liquid phase during solidification[6,7,13].

The effects of the stirring time were evaluated by processing the semisolid alloy at different stirring times: 1, 2, 4 and 8 minutes. Figure 5 shows the microstructures of the 6 mm samples processed at 595°C.

It can be noticed in Figure 5 that for longer stirring times the globular grains become coarser. The growth behavior of the globular grains is planar. Regarding the remaining interglobular region, it is possible to observe a refined globular morphology, refined dendritic structures and rosette-type structures. The liquid submitted to high cooling rates leads to a high nucleation rate and a refined structure. Due the nonuniformity of the mechanical stirring, some small solid particles can form rosette-like structures that are not completely round. The rosettes formation was also observed by other authors[12,17,25,26]. For longer stirring times, the small globules, projected in the remaining liquid region during processing, were incorporated by the larger globules during stirring time, refining the microstructure of the remaining interglobular region. At the same time, some particles remelted themselves into the superheated liquid[16].

For further analysis of the stirring time effects, the secondary dendritic arm spacing from the 6 mm diameter samples, comparing the different stirring times - 1, 2, 4 and 8 minutes - were measured in the remaining interglobular region (Table 2). The results showed that in the longest stirring times, 4 and 8 minutes, the remaining interglobular region became more refined, approximately 75% variation in regards to the first minute of stirring. Thus, this showed that the stirring time influences not only the primary α-Mg phase but also the interglobular region.

Table 2. Secondary dendritic arm spacing, obtained from the processed samples, for the different stirring times of 1, 2, 4 and 8 minutes, from 6 mm diameter sample.

Stirring time (minute)	SDAS (µm)	Standard deviation
CS	5.45	±0.40
1 min	19.46	±1.79
2 min	10.56	±4.08
4 min	5.03	±1.68
8 min	5.28	±2.28

3.4 Cooling rate analysis

The effects of the cooling rate on the microstructure of the processed samples were analyzed comparing the different diameter samples, 6 and 12 mm (Figure 6A-D),

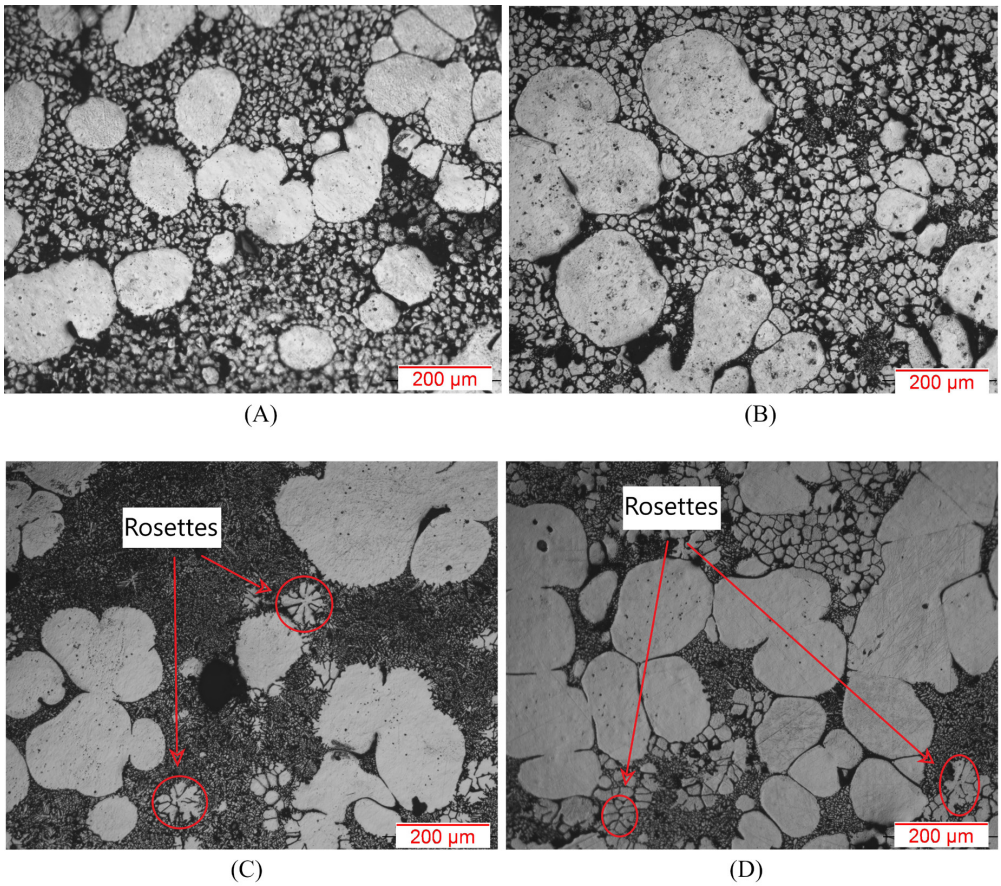

Figure 5. Evolution of the 6 mm samples processed at 595°C in different stirring times. (A) 1-minute; (B) 2-minutes; (C) 4-minutes and (D) 8-minutes.

rates of 371°C.s-1 ± 18 and 180°C.s-1 ± 13, respectively. A fixed stirring time (2 minutes) was stipulated for the comparison. It can be observed in Figure 6A and C that the different cooling rates did not significantly change the size or shape of the primary globular grains in the different diameters. In the images, it can be seen the large primary globular grains (α-Mg phase) dispersed in an interglobular region composed of refined dendrites and solute rich phases. In the interglobular structures (Figure 6B and D), a significant difference in the refinement is observed, which is related to the distinct cooling rates, but without significant differences in the size or shape of the dendritic or intermetallic phases. The interglobular structures, at the highest cooling rate, 6 mm sample (Figure 6A and B), became more refined and, at the lower cooling rate, 12 mm sample (Figure 6C and D) became coarser[8,21,22].

The secondary dendritic arm spacing measurements, performed in the interglobular region of the samples with different diameters (6 and 12 mm), showed that the SDAS is greater for samples with larger diameter and lower cooling rates, ranging from 17.90µm ±2.80 (12 mm) to 8.83µm ±1.99 (6 mm), with approximately 50% reduction. Therefore, the results showed that the primary α-Mg globular phase is much more affected by processing temperature and stirring time than by cooling rates. However, the different cooling rates directly affect the remaining interglobular region, refining the microstructure. This region is also affected by the stirring time, as shown earlier.

3.5 SEM and EDS analysis

From SEM micrographs (Figure 6) it is possible to see the primary α-Mg phase as well as the interglobular region. At the highest magnifications it is possible to see other phases present in the microstructure. Figure 6E shows the EDS results. Combining thermal analysis, SEM, EDS and results from the literature[12,23-27], the phases are probably as follows: the α-Mg primary phase, the Al-Ca rich phases Al_2Ca and $(Mg, Al)_2Ca$, presenting an irregular and coarse morphology, the Al_4Sr phase, with refined lamellar morphology, the Al_xMn_y phase, white particles dispersed in the primary and interglobular region, probably the Al_8Mn_5, $Al_{11}Mn_4$, Al_4Mn phases, and lastly, the $Ca_{2-x}Mg_xSn$ phase, with irregular shape dispersed in interglobular region.

3.6 Shape factor and mean grain size

Aiming at a better evaluation of the observed microstructural results, a correlation of the shape factor and the mean grain size of the primary globular phase was done with different stirring times and samples diameters. The results are expressed in Figure 7.

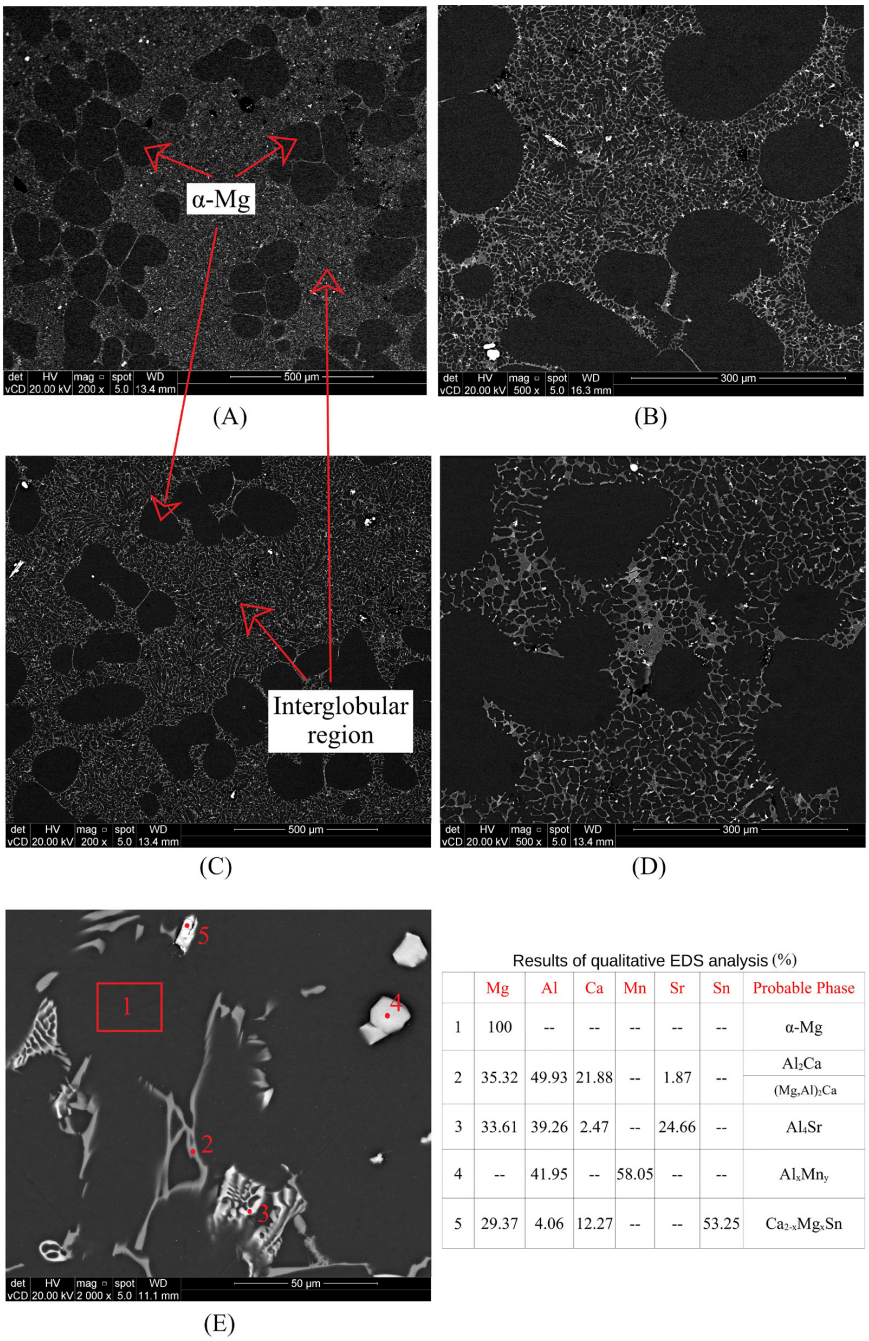

Results of qualitative EDS analysis (%)

	Mg	Al	Ca	Mn	Sr	Sn	Probable Phase
1	100	--	--	--	--	--	α-Mg
2	35.32	49.93	21.88	--	1.87	--	Al_2Ca / $(Mg,Al)_2Ca$
3	33.61	39.26	2.47	--	24.66	--	Al_4Sr
4	--	41.95	--	58.05	--	--	Al_xMn_y
5	29.37	4.06	12.27	--	--	53.25	$Ca_{2-x}Mg_xSn$

Figure 6. SEM micrographs comparing the processed samples with 6 and 12 mm diameter stirred for 2 minutes in different magnifications. (A) and (B) 6 mm; (C) and (D) 12 mm; (E) EDS Results.

The average shape factor of all diameters shows a tendency to increase with the increase of stirring time. The greatest increase occurred between 0 and 1 minute of stirring, stabilizing in the next minutes. However, due to the high standard deviation, it is not possible to make conclusions only with this analysis. To corroborate the SF results, mean grain size of the primary globular phase was measured (Figure 7B). The results showed that the mean grain size initially decreases after 1 minute of stirring when compared to the condition of not stirred. Then, it tends to increase with time. The initial behavior was compatible with the dendritic shear model, in which irregular primary α-Mg phase structure was sheared due to mechanical stirring, refining the microstructure and making it spherical, increasing the SF and reducing the grain size. The same occurred with the subsequent behavior, in which the larger globules grow at the expense of the smaller ones due to their lower global surface energy, forming a larger and more spherical primary phase with increasing time. The shape factor behavior continues until the moment when the growth becomes slower. The reduction in system

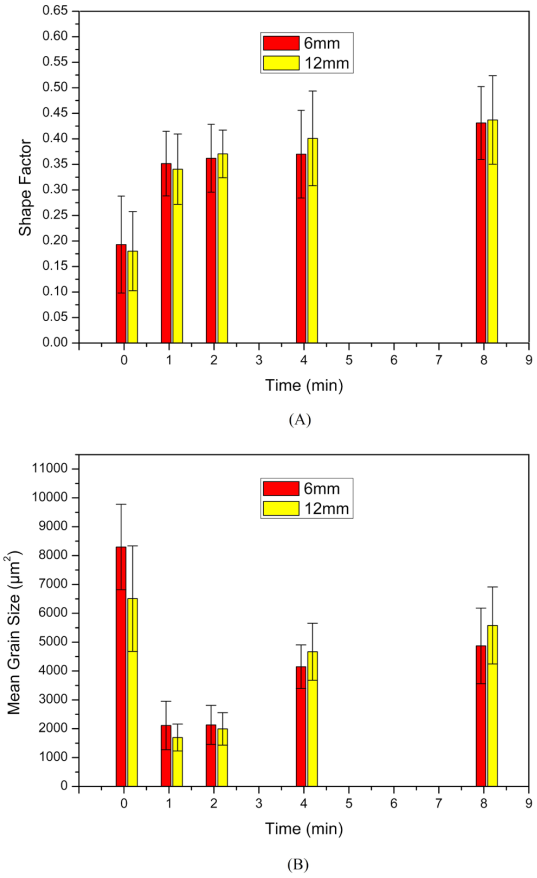

Figure 7. Results of the shape factor (A) and mean grain size (B) of the primary α-Mg phase in the samples processed at the different diameters and stirring times.

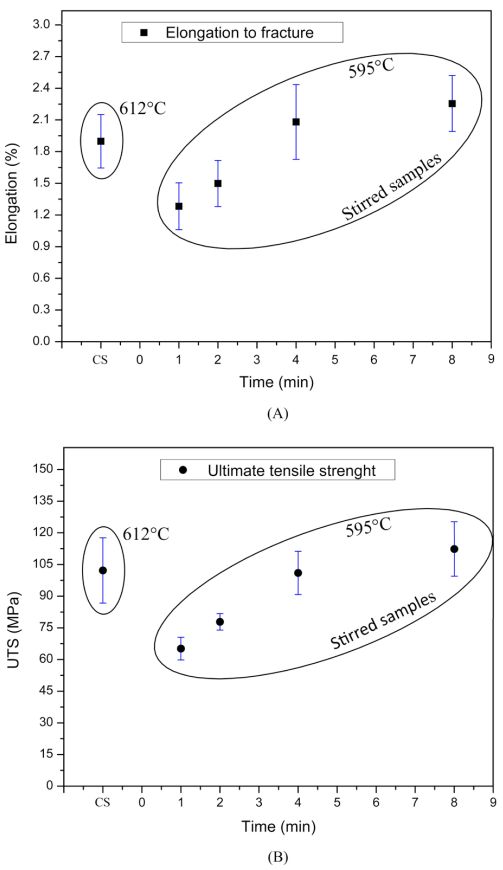

Figure 8. Elongation to fracture (A) and UTS (B) obtained from the tensile test at the different processing times and from the control sample (CS).

energy that occurred with the growth of the solid fraction slows down the process, forming some irregular particles and stabilizing the shape factor[6,16,20,28].

3.8 Mechanical tests

A comparative of elongation to fracture and ultimate tensile strength obtained in the tensile test at the different processing times and the control sample (CS) was done. Non-stirred samples, the CS samples collected at 612°C and the stirred samples processed at 595°C are presented. Figure 8 demonstrates the results of the 12 mm diameter samples.

The elongation to fracture, Figure 8A, shows an average reduction of approximately 1.9% to 1.2% comparing the sample CS with the 1-minute stirring sample. However, in the following minutes of stirring, it increased to approximately 2.2% of elongation in the 8-minute sample.

The ultimate tensile strength, Figure 8B, shows an average reduction of approximately 100 to 65 MPa between the samples CS and 1-minute stirring sample. However, it also increased in the following minutes reaching 112 MPa in the 8-minute sample.

An understanding of the morphology obtained in the processing is necessary, as the mechanical properties depend strongly on the size, solid fraction, shape factor and distribution of them. Besides that, assessments of tensile properties showed that the mechanical strength of magnesium alloys submitted to SSM processing are well compared, but not superior, to the die casting process, achieving better properties than conventional castings. In addition, they have higher ductility values, which have a strong dependence on the solid fraction[16,29].

Therefore, the initial reduction in the elongation to fracture between the non-stirred samples and 1-minute samples (CS and 1 min) may be related to the formation of shrinkage porosity on the samples, reducing its mechanical performance, unlike the CS samples that presented a refined and regular microstructure with no significant porosity. The subsequent increase in the elongation probably occurred due to the coalescence of the globular phase that directly influences ductility. The increase in the shape factor and a more regular distribution between the primary α-Mg grains and the interglobular region may also have influenced the mechanical performance. The UTS behavior was similar to the elongation: an initial reduction and a subsequent increase were observed. The initial behavior also may be related to the formation of shrinkage porosity, as well as the interglobular region presenting a coarser microstructure.

The subsequent increase occurred because of the refining of the interglobular region in the longest stirring times. The increase in the shape factor and a more regular distribution of the phases could also have influenced the results of the UTS. The shape factor improving both UTS and elongation is not fully understood. However, the results showed a tendency to behave similarly to that reported by ABDELGNEI et al. (2019), that the mechanical properties of Al-Si alloys have a strong dependence on the shape factor of the microstructure. The spherical shape has smaller interfacial grain area in comparison to other morphologies and, consequently, reduces the stress concentration formed in the interface between the primary and remaining phases. The same behavior is shown by other authors relating the shape factor of intermetallic structures to the increase in UTS[16,30-32]. This indicates that the relation between the microstructure of the primary globular phase and interglobular phases can positively affect the mechanical properties of the MRI 230D alloy, probably having an optimized point in the process.

Figure 9 shows the fracture surface of the slow cooling condition, obtained from the tensile test specimen, in different magnifications.

The fracture surface of Fig-9 revealed a coarse microstructure due to the slow cooling rate. It is possible to see mainly cleavage planes and grain boundaries, the details are indicated in the Fig-9 B and C. Therefore, the sample obtained in the slow cooling experiment presented a fragile fracture surface as well as transgranular and intergranular fractures. The relatively poor plasticity of magnesium alloys at room temperature is related to its hexagonal close-packed (HCP) structure with limited slip activity. The low number of independent sliding systems represents a limiting factor for plastic deformation of the HCP structure, especially at room temperature, as it does not satisfy the Von Mises criteria, which indicates that plastic deformations can happen if each crystal operates with a minimum of five independent sliding systems in order to activate and facilitate the sliding of the crystalline planes[2,33-35].

Figure 10 shows the fracture surface of the 12 mm sample, stirred for 2 minutes, obtained from the tensile test specimen in different magnifications. The processed sample presented a more refined microstructure when compared to slow cooling condition samples.

The fracture surface showed cleavage planes, indicated in the Fig-10C, as well as the detachment of the globules, indicated in the Fig-10B. Transgranular and intergranular fractures were observed. In small proportions, a plastic deformation in the grain boundaries, and in large proportion, a fragile deformation in the intergranular region were noted. Furthermore, it is possible to notice, in Fig-10C, the remaining dendritic interglobular region exposed. A lack of filling in the acquired samples (shrinkage porosity shown in Fig-4), ended up forming microcavities. Besides that, the interface decohesion directly occurred between solidified liquid fraction and the primary α-Mg phase. Magnesium alloys processed in a semi-solid state when submitted to

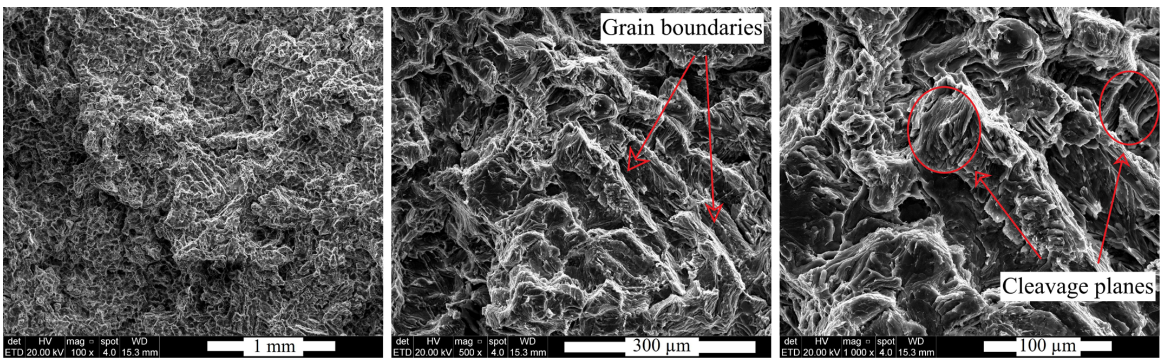

Figure 9. Fracture surface of the slow cooling condition.

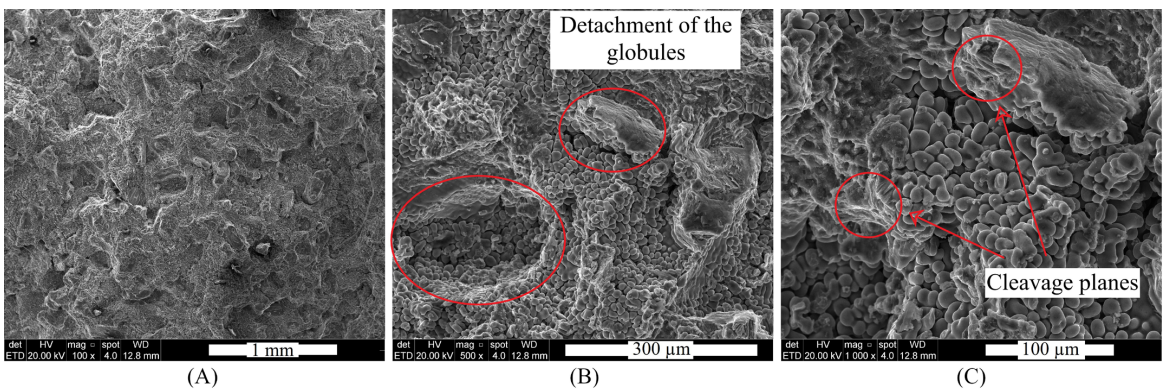

Figure 10. Fracture surface of the 12 mm sample mechanically stirred for 2 minutes.

tension will form a stress concentration at the interface of the primary and remaining phases. Crack propagation generally occurs in areas with stress concentration, thus affecting the mechanical performance of the material[2,33,35,36].

4. CONCLUSIONS

Mechanical stirring proved to be effective in obtaining a spherical structure in the MRI 230D alloy, with microstructural variation between the unprocessed and processed samples in the different parameters. The results showed that after 1 minute of stirring the globular structures begin to form. In longer periods of stirring, the globules tend to grow and have a higher shape factor.

The shape factor showed more significant differences in the first minute of stirring, as well as a more pronounced globular growth. In the following minutes of stirring there was a tendency to growth and, afterwards, to stabilize. Regarding the different cooling rates, the microstructure of the primary α-Mg phase did not show significant differences. However, as to the interglobular phases, there were differences in the refinement of its microstructure in approximately 50%. At higher cooling rates, a more refined microstructure was observed.

The results of the mechanical tests showed an initial reduction on the UTS, comparing the control sample (CS) and the processed samples. However, between 2 and 4 minutes of stirring, the material showed an increase. Thus, the highest UTS were obtained in the longest stirring times. The 8-minutes stirring samples resulted in an average ultimate strain of 112 MPa, a gain of approximately 12% when compared to the average of the CS samples, which reached 100 MPa. A similar result was observed on the elongation to fracture, with the best results for the longest stirring times, varying from 1.9% in the CS sample to 2.2% in the 8-minutes stirring samples, leading to a gain of approximately 16%. Therefore, the optimized rheocasting processing can generate not only a gain in ductility, but also in the mechanical strength of the MRI 230D alloy.

5. Acknowledgments

The authors acknowledge the Brazilian research agencies CAPES and CNPq for the financial support.

6. References

1. Tie D, Zhang B, Yan L, Guan R, Ji Z, Liu H, et al. Rheological solidification behavior and mechanical properties of AZ91-Sn alloys. Crystals (Basel). 2019;9(12):641.
2. Malik A, Yangwei W, Huanwu C, Khan MA, Nazeer F, Rui A, et al. Fracture behavior of twin induced ultra-fine grained ZK61 magnesium alloy under high strain rate compression. J Mater Res Technol. 2019;8(4):3475-86.
3. Mo N, Tan Q, Bermingham M, Huang Y, Dieringa H, Hort N, et al. Current development of creep-resistant magnesium cast alloys: a review. Mater Des. 2018;155:422-42. https://doi.org/10.1016/j.matdes.2018.06.032.
4. Guo HM, Zhang AS, Hu B, Ding Y, Liu XB. Refining microstructure of AZ91 magnesium alloy by introducing limited angular oscillation during initial stage of solidification. Mater Sci Eng A. 2012;532:221-9.
5. Yang X, Hou H, Zhao Y, Yang L, Han P. First-principles investigation of the structural, electronic and elastic properties of Al2Ca and Al4Sr phases in Mg-Al-Ca(Sr) alloy. J Wuhan Univ Technol Mater Sci Ed. 2014;29(5):1049-56.
6. Yim CD, Shin KS. Changes in microstructure and hardness of rheocast AZ91HP magnesium alloy with stirring conditions. Mater Sci Eng A. 2005;395(1-2):226-32.
7. Bartex SLT, Schaeffer L, De Barcellos VK. Morphological evolution of Mg-Al-La-Ca alloy induced by a mechanical stirring process. J Mater Eng Perform. 2019;28(7):3878-86. http://dx.doi.org/10.1007/s11665-019-03928-0.
8. Rasyid S, Arif E, Arsyad H, Syahid M. Effects of stirring parameters on the rheocast microstructure and mechanical properties of aluminum alloy ADC12. MATEC Web Conf. 2018;197. http://dx.doi.org/10.1051/matecconf/201819712004.
9. Zhang L, Wu G, Wang S, Ding W. Effect of cooling condition on microstructure of semi-solid AZ91 slurry produced via ultrasonic vibration process. Trans Nonferrous Met Soc. 2012;22(10):2357-63. http://dx.doi.org/10.1016/S1003-6326(11)61471-4.
10. Canyook R, Wannasin J, Wisuthmethangkul S, Flemings MC. Characterization of the microstructure evolution of a semisolid metal slurry during the early stages. Acta Mater. 2012;60(8):3501-10.
11. Terbush JR. Creep deformation in Mg-Al-Ca-based alloys [thesis]. Michigan (USA): University of Michigan; 2010. [cited 2020 Oct 12]. Available from: https://deepblue.lib.umich.edu/handle/2027.42/77917
12. Rzychoń T. Quantitative procedure for evaluation of microstructure of cast Mg-Al-Ca-Sr magnesium alloy. Arch Foundry Eng. 2010;10:139-42.
13. Zhang G, Qiu K, Xiang Q, Ren Y. Creep resistance of as-cast Mg-5Al-5Ca-2Sn alloy. China Foundry. 2017;14(4):265-71.
14. Gibbs JW, Mendez F. Solid fraction measurement using equation-based cooling curve analysis. Scripta Materialia, United States. 2008;58(8):699-702.
15. Bartex SLT, Dos Santos CA, De Barcellos VK, Schaeffer L. Effect of solid fraction on microstructures and mechanical properties of a Mg-Al-La-Ca alloy processed by rheocasting. J Alloys Compd. 2019;776:297-305.
16. Fan Z. Semisolid metal processing. Int Mater Rev. 2002;47(2):49-85.
17. Chen Y, Zhang L, Liu W, Wu G, Ding W. Preparation of Mg–Nd–Zn–(Zr) alloys semisolid slurry by electromagnetic stirring. Mater Des. 2016;95:398-409. http://dx.doi.org/10.1016/j.matdes.2016.01.131.
18. Esmaily M, Shahabi-Navid M, Mortazavi N, Svensson JE, Halvarsson M, Wessén M, et al. Microstructural characterization of the Mg–Al alloy AM50 produced by a newly developed rheo-casting process. Mater Charact. 2014;95:50-64. http://dx.doi.org/10.1016/j.matchar.2014.06.001.
19. Zhang Y, Wu G, Liu W, Zhang L, Pang S, Ding W. Effects of processing parameters on microstructure of semi-solid slurry of AZ91D magnesium alloy prepared by gas bubbling. T Nonferr Metal Soc. 2015;25(7):2181-7.
20. Farzam Mehr N, Aashuri H. The effects of annular electromagnetic stirring parameters on microstructure evolution of rheocastAZ91 magnesium alloy. J Mater Res Technol. 2019;8(2):2300-8. http://dx.doi.org/10.1016/j.jmrt.2019.03.009.
21. Reisi M, Niroumand B. Growth of primary particles during secondary cooling of a rheocast alloy. J Alloys Compd. 2009;475(1-2):643-7. http://dx.doi.org/10.1016/j.jallcom.2008.07.090.
22. Flemings MC. Coarsening in solidification processing. Mater Trans. 2005;46(5):895-900.
23. Janz A, Gröbner J, Schmid-Fetzer R. Thermodynamics and constitution of Mg-Al-Ca-Sr-Mn alloys: Part II. Procedure for multicomponent key sample selection and application to the Mg-Al-Ca-Sr and Mg-Al-Ca-Sr-Mn systems. J Phase Equilibria

Diffus, 2008;30(2):157-75. http://dx.doi.org/10.1007/s11669-009-9468-3.

24. Aljarrah M, Medraj M, Li J, Essadigi E. Phase equilibria of the constituent ternaries of the Mg-Al-Ca-Sr system [serial on the Internet]. JOM. 2009 [cited 2020 Oct 12];61:68-74. Available from: https://link.springer.com/article/10.1007/s11837-009-0075-x
25. Guan RG, Zhao ZY, Zhang H, Lian C, Lee CS, Liu CM. Microstructure evolution and properties of Mg–3Sn–1Mn (wt%) alloy strip processed by semisolid rheo-rolling. J Mater Process Technol. 2012;212(6):1430-6.
26. Wang C, Wu G, Sun M, Zhang L, Liu W, Ding W. Formation of non-dendritic microstructures in preparation of semisolid Mg-RE alloys slurries: roles of RE content and cooling rate. J Mater Process Technol. 2019;279:116545. https://doi.org/10.1016/j.jmatprotec.2019.116545.
27. Mondal AK, Kesavan AR, Ravi Kiran Reddy B, Dieringa H, Kumar S. Correlation of microstructure and creep behavior of MRI230D Mg alloy developed by two different casting technologies. Mater Sci Eng A. 2015;631:45-51. http://dx.doi.org/10.1016/j.msea.2015.02.037.
28. Wërz T, Baumann M, Wolfram U, Krill CE 3rd. Particle tracking during Ostwald ripening using time-resolved laboratory X-ray microtomography. Mater Charact. 2014;90:185-95.
29. Fang X, Lü S, Zhao L, Wang J, Liu L, Wu S. Microstructure and mechanical properties of a novel Mg–RE–Zn–Y alloy fabricated by rheo-squeeze casting. Mater Des. 2016;94:353-9.
30. Vaško A, Vaško M. Correlation between shape factor and mechanical properties of graphitic cast irons. Prod Eng Archives. 2016;11(2):11-4.
31. Yang L, Kang Y, Zhang F, Ding R, Li J. Rheo-diecasting of AZ91D magnesium alloy by taper barrel rheomoulding process. T Nonferr Met Soc. 2010;20(6):966-72. http://dx.doi.org/10.1016/S1003-6326(09)60243-0.
32. Abdelgnei MAH, Omar MZ, Ghazali MJ, Gebril MA. The effect of the Rheocast process on the microstructure and mechanical properties of Al-5.7Si-2Cu-0.3Mg alloy. Jurnal Kejuruteraan. 2019;31(2):317-26.
33. Wang Q, Bertolini R, Bruschi S, Ghiotti A. Anisotropic fracture behavior of AZ31 magnesium alloy sheets as a function of the stress state and temperature. Int J Mech Sci, 2019;163:105-43. http://dx.doi.org/10.1016/j.ijmecsci.2019.105146.
34. Yoo MH, Morris JR, Ho KM, Agnew SR. Nonbasal deformation modes of HCP metals and alloys: role of dislocation source and mobility. Metall Mater Trans, A Phys Metall Mater Sci. 2002;33(3):813-22. http://dx.doi.org/10.1007/s11661-002-0150-1.
35. Jiang L, Liu W, Wu G, Ding W. Effect of chemical composition on the microstructure, tensile properties and fatigue behavior of sand-cast Mg–Gd–Y–Zr alloy. Mater Sci & Eng: A. 2014;612:293-301. http://dx.doi.org/10.1016/j.msea.2014.06.049.
36. Chen Q, Yuan B, Lin J, Xia X, Zhao Z, Shu D. Comparisons of microstructure, thixoformability and mechanical properties of high performance wrought magnesium alloys reheated from the as-cast and extruded states. J Alloys Compd, 2014;584:63-75.